Journal of Materials Chemistry A

Accepted Manuscript

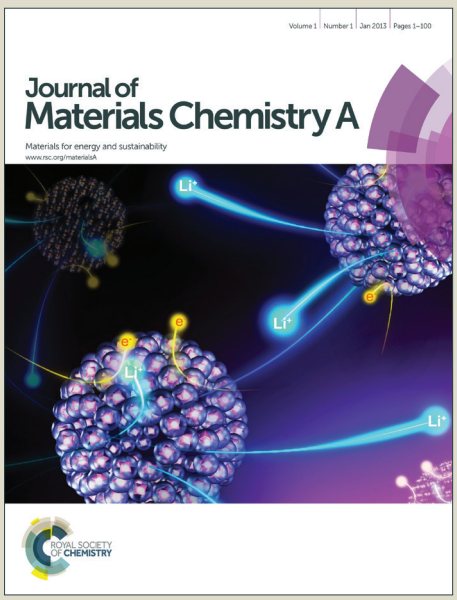

ROYAL SOCIETY OF CHEMISTRY

www.rsc.org/materialsA

Electrospun Nanofibers with Dual Plasmonic –Enhanced Luminescent Solar Concentrator Effects for High-Performance Organic Photovoltaic Cells

Jung-Yao Chen, [a] Yu-Cheng Chiu, [a] Chien-Chung Shih, [a]

Wen-Chung Wu, [b] and Wen-Chang Chen [a,*]

[a] Department of Chemical Engineering, National Taiwan University, Taipei, Taiwan 10617
Tel: 886-2-23628398, Fax: 886-2-23623040
E-mail:chenwc@ntu.edu.tw

[b] Department of Chemical Engineering, National Cheng Kung University
Tainan, Taiwan 70101
Tel: 886-6-2757575, Fax: 886-6-2344496
E-mail: wcwu@mail.ncku.edu.tw

We fabricated dual functional electrospun (ES) nanofibers by a coaxial electrospinning technique for enhancing organic photovoltaic device (OPV) efficiency, containing poly[2,7-(9,9-dihexylfluorene)-alt-4,7-(2,1,3-benzothiadiazole)](PFBT) nanoparticles as the luminescent solar concentrator (LSC) and Ag nanoparticles for the surface plasmon resonance (SPR) effect. The architecture of aligned- and cross-fiber patterns were fabricated to compare the architecture effects on the OPV efficiency. The plasmonic–enhanced LSC ES nanofibers within the crosslinked poly(methacrylic acid) could be directly integrated into the conventional OPV configuration without sacrificing the coverage area of active layer. In addition, the in-situ reduction of Ag nanoparticle simultaneously enhanced the exciton generation of PFBT and active materials with the SPR effect. The dual functional ES nanofibers with a crossed-pattern embedded into the OPV devices provided a significant light harvesting through down

conversion and enhanced exciton generation. They led to the PCE values of 4.11 and 7.12 % for P3HT (poly(3-hexylthiophene)):$PC_{61}BM$ ([6,6]-phenyl C_{61}-butyric acid methyl ester) and PTB7 (polythieno[3,4-b]-thiophene-co-benzodithiophene): $PC_{71}BM$([6,6]-phenyl C_{71}-butyric acid methyl ester) [6,6]-phenyl) photovoltaic cells, respectively, which were 18 % enhancement compared to their parent devices. This interface-modification approach using the plasmonic-enhanced LSC ES nanofibers provide a new approach for enhancing the OPV device performance.

Introduction

Organic photovoltaic devices (OPV) have attracted extensively scientific interest for renewable energy conversion due to the advantages of inexpensive, low fabrication temperature, and mechanical flexibility.[1-5] It is an essential concept to improve the optical thickness while keeping the physical thickness of bulk-heterojunction (BHJ) layer for harvesting sufficient incident photons, due to the comparatively low charge carrier mobility (usually less than 10^{-4} $cm^2V^{-1}s^{-1}$) of photo-active polymers. However, it remains a challenge using thin polymer film to create a more efficient light trapping and coupling environment for high performance OPV.[6]

Optical management strategies such as surface plasmon resonance (SPR) and luminescent solar concentrator (LSC) have been used to improve the OPV performance by enhancing light harvesting in the active layer.[7-15] For example, metallic nanostructures such as Au[3, 16-18] or Ag[13, 19]

were employed to improve the OPV power conversion efficiency (PCE) in a range of 10-25 % via the enhancement of localized surface plasmon resonance (SPR) effect. Besides, high optical concentration was also realized with LSC, consisted of specific fluorescent dye embedded in or coated on a transparent waveguide.[11, 20-25] In the device, the fluorescent dye absorbed in a low yield region and converted it into a spectral range suitable for the active layer. In addition, various device geometries had been provided to efficiently harness solar energy. For example, single- and tandem-waveguide organic solar concentrators with quantum efficiencies exceeding 50% could reduce the practical cost of photovoltaic power.[20] The dye-dispersed matrix in the inter-electrode gaps prolonged the stability but also substantially improved the shortcut current.[26] However, LSC usually located in the non-active zone which would significantly reduce the OPV area, especially for the device attached in the edge of LSC.[21] The down conversion layer was usually placed in front of a solar cell and resulted in the reflection loss at the air-down converter interface.[21] Besides, a main factor limiting LSC efficiency was the internal losses due to the overlap between the absorption and emission spectrum of dye.[26] Thus, reducing the cover area and self-absorption loss of LSC could be crucial for the practical applications.

Electrospinning (ES) is a versatile assembly method for fabricating uniform and ultrafine nanofibers with different patterning via various geometric collectors.[27-29] Also, ES nanofibers served as the matrix for functional materials such as metallic nanoparticles, conjugated polymers and quantum dots for diverse applications in optoelectronic devices.[30-32] The instinctive geometry

confinement provided by the nanofibers could manipulate the nanostructure and crystal orientation of constitutes. For example, the aggregation domain in the poly(9,9-dioctylfluoreny-2,7-diyl)/poly(methyl methacrylate) ES nanofibers was much smaller than that in the spin-coated film and it led to a higher photoluminescence efficiency.[33] Poly(vinyl alcohol) based ES nanofibers embedded with controlled alignment of silver nanoparticles produced the SPR effect to 4-mercaptobenzoic acid molecules with an enhancement factor of 10^9.[34] Au nanorods were incorporated into poly(acryl amide) uniaxially-aligned ES fibers for optical waveguiding applications with photon-to-plasmon conversion efficiency of 70 %.[31] Nevertheless, the integrated dual functions of SPR and LSC effects in ES nanofibers for enhancing BHJ OPV device performance have not been reported yet, to the best of our knowledge.

In this study, ES nanofibers consisted of poly[2,7-(9,9-dihexylfluorene)-alt-4,7-(2,1,3-benzothiadiazole)](PFBT)/Ag/Poly(methacrylic acid)(PMAA) were fabricated and embedded in the OPV devices using the active layer of P3HT (poly(3-hexylthiophene)):$PC_{61}BM$ ([6,6]-phenyl C_{61}-butyric acid methyl ester) or PTB7 (polythieno[3,4-b]-thiophene-co-benzodithiophene):$PC_{71}BM$([6,6]-phenyl C_{71}-butyric acid methyl ester) [6,6]-phenyl), as shown in **Fig. 1**. The effect of aligned or crossed-fiber pattern on the OPV characteristics were explored. PFBT and Ag nanoparticles served as the LSC and SPR effects, respectively. The dual functional ES nanofibers with two light harvesting materials were

produced with the core-sheath electrospinning technique. The in-situ reduction of Ag nanoparticles simultaneously enhanced the exciton generation of PFBT and the active layer with the SPR effect. The crosslinked PMAA provided an solvent-resistant matrix for LSC without changing the conventional OPV configuration. Our dual functional nanofibers presented a new approach to enhance the OPV devices with the combination of two light trapping effects (SPR and LSC) and the maintenance of active area coverage.

Experimental Section

Materials

PFBT was synthesized using Suzuki coupling reaction reported previously,[35] with the number-average molecular weight (M_n) and polydispersity index of PFBT of 5360 and 1.68. Silver nitrite ($AgNO_3$, TCI (Tokyo, Japan)), poly(methacrylic acid)) (PMAA) (Mv ~ 180,000, Scientific Polymer Products, USA), tetrahydrofuran (THF), dimethylformamide(DMF), ethyl glycol (EG, anhydrous, 99%) and diiodooctane (DIO) were purchased from Sigma-Aldrich (Missouri, USA) and used as received. P3HT (Mw ~50,000, 90-95 % regioregular, Reike Metals Inc. (Lincoln, NE)), PTB7 (Mw>50,000, Lumtec, Taiwan), $PC_{61}BM$ (99.7%, Nano-C (Massachusetts, USA)) and $PC_{71}BM$ (99.7%, Nano-C (Massachusetts, USA)) were used without further purification.

Preparation of LSC-SPR Electrospun Nanofibers

A two-fluid coaxial ES technique with a modified collector was employed to produce core/shell nanofibers, similar to our previous report.[28,36] Two syringes containing core and shell solutions were connected to a separate needle, and the needle was placed one inside the other to form a two-fluid coaxial ES system. The core and shell polymeric solutions were fed into the coaxial capillaries by two syringe pumps (KD Scientific Model 100, USA). The feed rate of core flow was fixed at 0.1 ml h^{-1} while the shell flow was operated at 1.0 ml h^{-1} for all of the ES nanofibers. The tip of the core needle was connected to a high-voltage power supply (chargemaster CH30P SIMCO, USA). The spinning voltage was set at 14-15 kV and the working distance (the distance between tip of the needle and collector) was fixed at 13 cm. The stable cone-jet spinning mode in the ES process was monitored by a CCD camera (XLi 3M USB2.0 CCD camera, USA) and Macro video zoom lens (OPTEM MVZL, USA) for obtaining uniform and aligned nanofibers. All ES experiments were carried out in air. The nanofibers can be stretched across the collector gap (4 cm in length and gap width of 1 cm) to form a parallel array and crossed pattern by transferring two layers of uniaxially aligned composite nanofibers onto the same substrate, as shown in **Fig. 1**.

Preparation of PFBTNF-LO and PFBTNF-HI LSC nanofibers: First, the PFBT nanoparticles was prepared through reprecipitation. 0.4 mg mL^{-1} of PFBT was dissolved in THF and then dropwise precipitated into a poor solvent (H_2O/DMF = 1:1) under 50 ℃ to

evaporate THF.[37] In the following, 220 mg mL^{-1} of PMAA was dissolved in above solution contained 0.144 mg mL^{-1} (named as PFBTNF-LO) or 0.288 mg mL^{-1} (named as PFBTNF-HI) PFBT nanoparticles as the shell solution. With the help of EG as crosslinker in the core part, the crosslinked nanofiber could be produced after thermal treatment at 200 °C. [9, 38]

Preparation of the AgNF SPR nanofibers: 300 mg mL^{-1} $AgNO_3$ dissolved in EG as the core solution and 220 mg mL^{-1} of PMAA dissolved in H_2O/DMF mixed solvent as shell solution. The as-spun nanofibers were further annealed at 200 ^oC for 20 min to reduce Ag ion under the help of EG and named as **AgNF**.

Preparation of LSC-SPR dual function nanofibers: PFBT-LO/AgNF and PFBT-HI/AgNF ES nanofibers were obtained using 300 mg mL^{-1} $AgNO_3$ dissolved in EG as the core solution and PFBT nanoparticles/PMAA dissolved in H_2O/DMF mixed solvent as the shell solution which contained 0.144 mg mL^{-1} or 0.288 mg mL^{-1} PFBT nanoparticles, respectively. The further thermal treatment at 200 ^oC for 20 min simultaneously reduced the Ag ion and crosslinked the PMAA through the help of EG, which served as solvent, reducing agent and crosslinker.

Characterization

The material characterizations of PFBT are described in the following: ^1H nuclear magnetic resonance (NMR) spectrum wwas obtained using a Bruker Avance DRX-400 MHz

spectrometer. The size exclusion chromatography (SEC) was performed at 40 ℃ in THF (1.0 mL min^{-1}) using a JascoGPC-900 system equipped with set of Waters Ultrastyragel 7 mm columns (linear, 7.8 mm × 300 mm) and two Shodex KF-804 L columns (linear, 8 mm × 300 mm). The M_n and polydispersity index were calculated on the basis of polystyrene standards. The morphology of the studied nanofibers was characterized by the following instruments: Field-emission scanning electron microscope (FE-SEM) images were taken using a microscope (JEOL JSM-6330F) operated at an accelerating voltage of 10 kV. Fluorescence optical microscope images were obtained using a two photon laser confocal microscopes (Confocal) (Leica LCS SP5). Time-resolved photoluminescence (TRPL) spectroscopy was performed with a time-correlated single photon counting (TCSPC) spectrometer (Picoquant, Inc.). A pulse laser (380 nm) with an average power of 1 mW operating at 1 MHz for 260 ns was used for excitation. UV-Visible absorption spectra and steady-state photoluminescence (PL) spectra were recorded on a Hitachi U-4100 spectrophotometer and Horiba Fluorolog-3 spectrofluorometer (Jobin Yvon), respectively. Transmission electron microscope (TEM) images and selected-area electron diffraction (SAED) pattern were taken using a microscope (FEI Tecnai G2 20) operated at 200 keV to observe the distribution and crystallographic orientation of nanostructural Ag particles in the prepared AgNF. Atomic force micrographs were obtained with a Nanoscope 3D Controller

AFM (Digital Instruments, Santa Barbara, CA) operated in the tapping mode at room temperature.

Electrical Characterization of AgNF

To measure the two-terminal resistances of AgNF, aligned composite nanofibers were prepared from the above ES process and deposited on the silicon wafer with a 200 nm-thick SiO_2 layer. Note that the wafer was first cleaned with toluene, acetone, and isopropyl alcohol, and then dried by a N_2 steam. Top-contact electrodes were defined by 100 nm-thick of Au through a regular shadow mask with channel length of 2.5 mm. The electrical conductivity of the nanofibers was calculated from the slope of the current (*I*)-voltage (*V*) curve using a Keithley 4200-SCS semiconductor parameter analyzer (Keithley Instruments Inc., Cleveland, OH, USA), with a remote PreAmp (4200-PA) in a N_2-filled glove box at room temperature. The scanning voltage was applied from -50 V to 50 V with the stepwise of 1 V.

Fabrication and Characterization of Photovoltaic Cells using the ES composite Nanofibers

All the bulk-heterojunction photovoltaic cells were prepared using the same procedures, as described in the following. The glass-indium tin oxide (ITO) substrates (obtained from Luminescence Technology Corp., Taiwan, 7 Ω sq^{-1}) were first patterned by a lithographic

process, then cleaned with detergent, and ultrasonicated in acetone and isopropyl alcohol, then subsequently dried on a hot plate at 120 °C for 5 min. ES nanofibers deposited on the ITO substrate using the rectangular metal gap to prepare the aligned and crossed fiber patterns as shown in **Fig. 1**. Poly(3.4-ethylenedioxy-thiophene):poly(styrene-sulfonate) (PEDOT:PSS, Baytron P VP AI4083) passed through a 0.45 μm filter and then spin-coated at 3500-5000 rpm on ITO/nanofibers and dried at 140 ^{o}C for 20 min under an ambient environment. The active layer of the P3HT:$PC_{61}BM$ blend (1:0.8, w/w) in anhydrous DCB (17.5 mg mL^{-1}) was followed by spin-coating at 1000 rpm on top of the PEDOT: PSS layer. These as-cast film was kept in petri dish to control the drying rate under a nitrogen atmosphere. After that, the device was annealed at 140 ^{o}C for 10 min in a N_2-filled glove box. For the PTB7/$PC_{71}BM$ photovoltaic cells, 10 mg mL^{-1} PTB7 and 15 mg mL^{-1} $PC_{71}BM$ were dissolved in CB with 3% DIO to promote the morphology. The above solution was followed by spin-coating at 1000 rpm on top of the PEDOT: PSS layer for 2 min and then treated with Methanol for 1 min to remove impurity. Subsequently, the device was deposited Ca (30 nm) and Al (100 nm) by thermal evaporation under a high vacuum ($<10^{-6}$ torr) with the active area of 4 mm^2. The current density (*J*)-voltage (*V*) measurement of the photovoltaic devices was conducted by a computer-controlled Keithley 2400 (Keithley Instruments Inc., Cleveland, OH, USA) source measurement unit (SMU) with a Peccell solar simulator under the illumination of AM 1.5 G, 100 mW cm^{-2}. The illumination intensity was calibrated by a standard Si photodiode detector

with KG-5 filter. In addition, the external quantum efficiency (EQE) was measured by using a Xe lamp in combination with a monochromator (Oriel Inc., USA).

Results and Discussion

Morphology and Photovoltaic Characteristics using LSC Nanofibers

Fig. 1 shows the schematic diagram of the coaxial ES process to prepare three kinds of electrospun nanofibers, PFBTNF, AgNF and PFBT/AgNF, with the aligned- or crossed- fiber pattern. The prepared LSC nanofibers with the low and high PFBT compositions are named as PFBTNF-LO and PFBTNF-HI, respectively. In addition, the aligned (A-)and crossed (C-) fiber pattern were used to probe the pattern effects toward OPV performance, denoted as C-PFBTNF-LO, A-PFBTNF-HI and C-PFBTNF-HI, respectively .

By precisely controlling the solvent polarity, the PFBT nanoparticles with the average diameter of 13.33± 4.18 nm could be obtained by precipitation through the process of dissolving in a good solvent, THF, and then slowly dropping into a poor mixed solvent (H_2O: DMF =1:1) (**Fig. S1** of the ESI†). Through the Főrster energy transfer between 9,9-dihexylfluorene (F) and 2,1,3-benzothiadiazole (BT), PFBT shows a high stock-shift characteristic and suppresses the reabsorption loss.[35] PFBT is chosen to absorb the low yield region of the BHJ (300-450 nm) and subsequently emit a spectral range suitable for the absorption of BHJ (450-650 nm) through Főrster energy transfer,[20] as shown in **Fig. 2**.

Fig. 3 shows the SEM images of the nonwoven PFBTNF-HI treated with different crosslinking time and subsequently immersing into water (the good solvent for PMAA) to confirm the degree of crosslinking. With 5 min crosslinking, PFBTNF-HI shows a flatted structure (**Fig. 3a**) after being extracted by water. By extending the crosslinking time to 10 min, the ES nanofibers could maintain a cylindrical shape but still tend to stick together, as shown in **Fig. 3b**. After crosslinking for 20 min, the solvent-resistant cylindrical ES nanofibers with the average diameter of 550 nm are obtained even though immersed in water for 20 min (**Fig. 3c**). Meanwhile, the hydrophilic property of PMAA exhibits a high adhesion with indium tin oxide (ITO) which keeps the pattern intact. Through precisely controlling the concentration of the PFBT solution and the volume of the mixed solvent, the evenly-distributed nanoparticles within the nanofibers are obtained. The TEM image shows that the PFBT nanoparticles are well-dispersed in PFBTNF-HI with an uniform size around 5 nm, as shown in **Fig. 4a**, which is consistent with the SEM image (**Fig. S1 of the ESI**[†]).

Furthermore, the patterned LSC ES nanofibers were incorporated into the OPV devices with the sandwich configuration of ITO/nanofibers/PEDOT:PSS/active layer/Ca/Al, as shown in **Fig. 5**. The corresponding current density (J)-voltage (V) characteristics of the devices with PFBTNF-LO and PFBTNF-HI are illustrated in **Fig. 6**, and summarized in **Table 1**. For the P3HT:$PC_{61}BM$ photovoltaic cells, the controlled cell without the ES nanofibers reaches a PCE of 3.49 % with the open circuit voltage (V_{oc}) of 0.63 V, short circuit current (J_{sc}) of 8.21

mA cm^{-2}, and fill factor (FF) of 0.675. The PCE of the devices with the aligned nanofibers shows an obvious improvement from 3.49 % (the reference cell) to 3.70 % (A-PFBTNF-LO) and 3.96 % (A-PFBTNF-HI) with the J_{sc} values of 8.21, 8.92, and 9.40 mA cm^{-2}, respectively. This improvement in J_{sc} is attributed to the down conversion effect of PFBT, which exhibits a high stock-shift characteristic through Főrster energy transfer to suppress the reabsorption loss. That is, the cylindrical LSC embedded in the OPV effectively absorbs the low absorption region (300-450 nm) and radially re-emits a spectral range similar to the absorption of the active layer (450-600 nm). However, the device performance using the embedded C-PFBTNF-HI crossed-fiber pattern is similar to that of the controlled cell (**Table S1** and **Fig. S2** of the ESI†). The relative higher series resistance (*R*s) in the crossed-fiber pattern is probably resulted from the high variation on the vertical altitude and it hinders the formation of a smooth film. To futher elucidate the decreased PCE of the OPV devices with the LSC crossed-fiber pattern compared to that of the aligned-fiber pattern, the surface structure of the P3HT:PC_{61}BM active layer was analyzed by AFM. The obvious difference between the two patterns is that the fused joint originates from two nanofibers crossed each other. Estimated from the cross-section analyses of the AFM images (**Fig. S3** of the ESI†), the single and fused nanofibers coated with PEDOT:PSS/ P3HT:PC_{61}BM show different vertical altitude of 103 nm and 166 nm, respectively. Simultaneously, the roughness would be gradually increased from 1.71 to 3.96 nm for the P3HT:PC_{61}BM layer near single and fused fibers. The higher

vertical altitude change from the fused joint of nanofibers probably accounts for the higher surface roughness of the active layer near the nanofibers, leading to deterioration of the device performance. Note that the C-PFBTNF-HI is a nonconductive nanofiber which could not reduce the bulk resistance of device through crossed-fiber pattern as our previous report[2] and sacrifice the light trapping effect instead. Thus, the PCE of the photovoltaic device using C-PFBTNF-HI is lower than that of A-PFBTNF-HI, due to its higher surface roughness.

Morphology and Phtovoltaic Characteristics using SPR ES Nanofibers

The core and shell solutions of $AgNO_3$ in EG and PMAA in H_2O/dimethylformamide(DMF) mixed solvent were used to prepare the the AgNF with the SPR effect, where EG was the reducing agent for forming Ag nanoparticles. Note that the theoretical weight percent of Ag in AgNF is 8 wt. % based on the total fiber weight. Besides, only the crossed-fiber pattern of AgNF was implemented here because of its higher conductivity compared to the aligned one as our previous report,[2] leading to a higher PCE.

As shown in our previous report,[2] coaxial core-sheath ES technique with the Ag precursor and shell polymer as core and shell solutions, respectively could be employed to prepare the highly conducting Ag-contained nanofibers with a SPR effect. The exciton generation of the active layer is increased by the presence of Ag nanoparticles; however, they could also function as traps for the polarons in its locality.[39] Therefore, Ag nanoparticles covered by dielectric materials would be an essential tactic for suppressing the contact with the active

layer. In this study, Ag-contained nanofibers, named as AgNF, was utilizing $AgNO_3$ dissolved in EG as the substitute of $Ag(NH_3)_2^+$ and PMAA as shell polymer for crosslinking.

To track the Ag reduction as well as morphological evolution in the AgNF textiles, UV-visible absorption spectra were performed since different shapes of Ag nanostructures exhibited the SPR bands at variant frequencies.[40] As shown in **Fig. 7a**, there is a broad signal indicating the silver ions could be effectively reduced by EG, even though the as-spun nanofibers are stored under room temperature.[27] The intensity of SPR signal abruptly increases after the AgNF annealed at 200 ^oC, showing more Ag ions are reduced and the Ag nanoparticles are growing with an increased annealing time. It indicates that the Ag nanoparticles embedded plasmonic ES nanofibers can be directly manufactured via thermal treatment. Besides, the broadband SPR signal of AgNF, ranging from 300 to 700 nm, illustrated its broad wavelength range for absorption enhancement. The inset Fig. shows the SAED of the corresponding AgNF. The ring pattern indicates the crystallinity of Ag nanoparticle is lower than that of our previous Ag/polyvinylpyrrolidone (PVP) ES nanofibers.[2] It has been reported that PVP with nitrogen can form the N-Ag coordinating bond which suppress the growth of {100} facets through the selectively absorption and desorption.[41] However, the carboxylic acid group of PMAA may form a strong intramolecular hydrogen bond which inhibits the oxygen interacting with the Ag surface and, thus, form amorphous silver nanoparticles.[42] In **Fig. 4b**, TEM image shows that Ag nanoparticles in

AgNF have a diameter of 4 nm and uniformly disperse within nanofibers. It indicates that the in-situ reduction of Ag nanoparticles can be fully covered by the PMAA for fear of the direct contact with active layer during the following OPV fabrication. Furthermore, the electrical characteristic of the AgNF was performed using a two-terminal electrical measurement. **As** shown in **Fig. 7b**, the nonlinear *I-V* curve of AgNF at the lower bias is probably resulted from that the inter-grain boundary of Ag nanoparticles or the PMAA component blocks the electron transportation in a low voltage bias,[2, 43] but the nanofibers become conductive at a higher bias. The calculated conductivity of AgNF is 4.48×10^5 S m^{-1} similar with our previous report,[2] which can effectively reduce the bulk resistance of OPV. Compared to the reference device, P3HT:PC_{61}BM OPV device using the C-AgNF crossed- pattern nanofiber shows an improvement in the PCE (3.84 %) and J_{sc} (8.82 mA cm^{-2}) due to the high conductivity and the SPR effect, similar to our previous report.[2] The detail OPV performance and the corresponding current density (*J*)-voltage (*V*) characteristics of the devices also show in **Fig. 6** and **Table 1**.

Morphology and Photovoltaic Characteristics Using Dual LSC/SPR Function Nanofibers

The LSC and SPR dual functions of nanofibers, crossed-fiber pattern C-PFBT-LO/AgNF and C-PFBT-HI/AgNF were fabricated through the coaxial ES system with PFBT

nanoparticles/PMAA as shell and $AgNO_3$ dissolved in EG as core, while the algined dual function nanofiers, A-PFBT-HI/AgNF, was also prepared for comparison. Combination of two light harvesting strategies (LSC, SPR) could be realized through the coaxial ES system using PFBT and Ag nanoparticles, respectively, as the morphology confirmed by the TEM image (**Fig. 5c**). Both the PFBT and Ag nanoparticles retained the original sphere shape and well-dispersed in the ES nanofiber. The emission properties of fluorescence molecules could be strongly modified when they surrounded by metal nanostructure.[9, 44, 45] To probe the plasmonic-enhanced PL of the PFBT, PL measurement is not feasible due to the difficulty in the quantitative collection of ES nanofibers. A complementary approach using confocal image of a single nanofiber was performed instead. **Fig. 8a and 8b** shows the confocal images of PFBTNF-HI and PFBT-HI/AgNF. As shown in the above TEM image (**Fig. 4a**), the nanofibers composed of PFBT nanoparticles result in discretely fluorescent spheres in the confocal image. The PL intensities on two different kinds of nanofibers, PFBTNF-HI and PFBT-HI/AgNF, are 14.81 a.u. and 29.01 a.u., respectively, while the corresponding quantum yields are 27.5 and 31.4 %, respectively. Furthermore, to elucidate the effect of silver nanoparticles on the LSC nanofibers, the recombination kinetics of the PFBT exciton through time-resolved PL (TRPL) are examined, as shown in **Fig. 8c**. All profiles could be fitted to single exponential decay functions to obtain the exciton lifetimes (τ). The fitted lifetime of PFBTNF-HI is 2.74 ns and it decreases to 2.3 ns for PFBT-HI/AgNF after surrounded by

silver nanoparticles. It suggests that the coupling between the plasmons and excitons leads to an increased exciton recombination rate. The Ag-contained ES nanofibers of PFBT-HI/AgNF provides the SPR effect not only for the PFBT but also the P3HT:PC_{61}BM film. UV-Visible absorption and corresponding enhancement ratio of the P3HT:PC_{61}BM active layer with or without Ag-contained ES nanofiber were used to elucidate the SPR effect for active layer, as shown in **Fig. 9a**. The spectrum shows that the absorption intensity of the active layer with C-PFBT-HI/AgNF is enhanced over the whole range compared to the pristine P3HT:PC_{61}BM. Besides, the emission intensities of P3HT:PC_{61}BM film after incorporating the C-AgNF and C-PFBT-HI/AgNF are also enhanced, as shown in **Fig. 9b**. The significant change on the PL intensity of the P3HT:PC_{61}BM film suggests the energy transfer between the Ag and photo-active layer. Such metal-enhanced fluorescence further suggests the role of the SPR in the enhanced exciton generation of P3HT:PC_{61}BM.

The OPV devices using plasmonic–enhanced ES nanofibers, C-PFBT-LO/AgNF and C-PFBT-HI/AgNF crossed-pattern nanofibers, exhibit the PCEs of 3.98 and 4.11 % with the J_{sc} values of 9.43 and 9.45 mA cm^{-2}, respectively, leading to remarkably 18 % enhancement on the PCE. It is worth to mention that the device with Ag-contained nanofiber (C-PFBT-HI/AgNF) show better OPV performace in crossed pattern compared to those in the aligned one (A-PFBT-HI/AgNF), which is contrast to the result of the device with the nonconductive PFBTNF-HI. Note that the V_{oc} (generally 0.63 V) and FF (in a range of 0.67 to

0.68) of all nanofibers-containing OPVs show an insignificant difference. Thus, the increase of PCE is mainly attributed to the improvement of J_{sc} from the plasmonic-enhanced LSC ES nanofibers.

These plasmonic-enhanced LSC ES nanofibers can also be implemented for the high PCE photovoltaic cell using the PTB7:$PC_{71}BM$ as active layer. After incorporating PFBTNF-LO and PFBTNF-HI into the photovoltaic cells, the PCE improves from 6.05% to 6.31 and 6.55 % with the J_{sc} values of 12.75 and 12.84 mA cm^{-2}, respectively. Moreover, the OPV devices with C-AgNF, C-PFBT-LO/AgNF and C-PFBT-HI/AgNF exhibit the PCE values of 6.44, 6.63 and 7.12 % with the J_{sc} values of 12.91, 13.04, and 13.88 mA cm^{-2}, respectively. The above results indicate that the plasmonic-enhanced LSC ES nanofibers are a promising candidate for enhancing the OPV device performance.

Fig. 9c shows the external quantum efficiency (EQE) results of the studied P3HT:$PC_{61}BM$ OPV devices using the prepared ES nanofibers. The EQE values of all OPV devices are increased after employing the C-AgNF and C-PFBT-HI/AgNF with covered a wide-range wavelength from 300 to 800 nm. Furthermore, the integrated photocurrent densities from the EQE spectrum of the reference, C-AgNF and C-PFBT-HI/AgNF are 8.27, 8.80 and 9.47 mA cm^{-2}, respectively. The enhancement is a consequence of the improved charge carrier mobility, light harvesting from LSC and the enhanced exciton generation rate due to the SPR effect from the studied ES nanofibers. All the integrated current density values are in a good

agreement with the measured photocurrent densities (within 5 % error), indicating that the obtained photovoltaic characteristics are reliable. Note that the EQE enhancement have highly-enhanced absorption region located at the 600~800 nm, which is consistent with the UV-Visible absorption characteristics. The dual functional ES nanofibers also can be implemented for PTB7:$PC_{71}BM$ OPV devices with the proof of EQE results (**Fig. S4** of the ESI†).

Conclusion

We have successfully prepared plasmonic-enhanced LSC ES nanofibers using the coaxial electrospinning technique with PFBT and Ag nanoparticles for LSC and SPR effects, respectively. The ES nanofiber matrix, crosslinked PMAA, provides a solvent-resistant matrix for plasmonic-enhanced LSC ES nanofibers without changing the conventional OPV configuration. Besides, the in-situ reduction of Ag nanoparticles simultaneously enhanced the exciton generation of PFBT and active material with the SPR effect. The dual functional ES nanofibers allow significant light harvesting and exciton generation, leading to remarkably 18 % enhancement on the PCE for both P3HT:$PC_{61}BM$ and PTB7: $PC_{71}BM$ photovoltaic cells. The developed dual functional nanofibers provide a novel approach to integrate the plasmonic-enhanced LSC ES nanofiber into the OPV device with the combination of two light trapping methods (SPR and LSC) and the maintenance of active area coverage.

Acknowledgements

This work was financially supported by the grant from the Ministry of Science and Technology, Taiwan. The authors thank Mr. Ying-Chiao Wang, Mr. Chi-Huang Chang, and Prof. Chun-Wei Chen in Department of Materials Science and Engineering, National Taiwan University, for facilitating the TRPL and EQE experiments. Besides, we also gratefully acknowledge the Instrumentation Center (sponsored by Ministry of Science and Technology, Taiwan) and Technology Commons in College of Life Science, National Taiwan University for the confocal experiment.

Notes and references

†Electronic Supplementary Information (ESI) available. See DOI: 10.1039/b000000x/

1. S. Guenes, H. Neugebauer and N. S. Sariciftci, *Chem. Rev.*, 2007, **107**, 1324-1338.
2. J.-Y. Chen, H.-C. Wu, Y.-C. Chiu and W.-C. Chen, *Adv. Energy Mater.*, 2014, **4**, 1301665.
3. X. Yang, C.-C. Chueh, C.-Z. Li, H.-L. Yip, P. Yin, H. Chen, W.-C. Chen and A. K. Y. Jen, *Adv. Energy Mater.*, 2013, **3**, 666-673.
4. Z. He, C. Zhong, S. Su, M. Xu, H. Wu and Y. Cao, *Nat Photon*, 2012, **6**, 591-595.
5. J.-S. Wu, S.-W. Cheng, Y.-J. Cheng and C.-S. Hsu, *Chem. Soc. Rev.*, 2015, **44**, 1113-1154.
6. D.-H. Ko, J. R. Tumbleston, A. Gadisa, M. Aryal, Y. Liu, R. Lopez and E. T. Samulski, *J. Mater. Chem.*, 2011, **21**, 16293-16303.
7. H. Choi, S.-J. Ko, Y. Choi, P. Joo, T. Kim, B. R. Lee, J.-W. Jung, H. J. Choi, M. Cha, J.-R. Jeong, I.-W. Hwang, M. H. Song, B.-S. Kim and J. Y. Kim, *Nat Photon*, 2013, **7**, 732-738.
8. E. Hutter and J. H. Fendler, *Adv. Mater.*, 2004, **16**, 1685-1706.
9. H. A. Atwater and A. Polman, *Nat Mater*, 2010, **9**, 205-213.
10. C.-C. Chueh, C.-Z. Li and A. K. Y. Jen, *Energ. Environ. Sci.*, 2015 DOI: 10.1039/c4ee03824j.
11. T. F. Schulze and T. W. Schmidt, *Energ. Environ. Sci.*, 2015, **8**, 103-125.
12. W. Cao and J. Xue, *Energ. Environ. Sci.*, 2014, **7**, 2123-2144.

13. S.-J. Ko, H. Choi, W. Lee, T. Kim, B. R. Lee, J.-W. Jung, J.-R. Jeong, M. H. Song, J. C. Lee, H. Y. Woo and J. Y. Kim, *Energy & Environ. Sci.*, 2013, **6**, 1949-1955.
14. F.-x. Xie, W. C. H. Choy, W. E. I. Sha, D. Zhang, S. Zhang, X. Li, C.-w. Leung and J. Hou, *Energ. Environ. Sci.*, 2013, **6**, 3372-3379.
15. D. C. Lim, B. Y. Seo, S. Nho, D. H. Kim, E. M. Hong, J. Y. Lee, S.-Y. Park, C.-L. Lee, Y. D. Kim and S. Cho, *Adv. Energy Mater.*, 2015, DOI: 10.1002/aenm.201500393.
16. J. Yang, J. You, C.-C. Chen, W.-C. Hsu, H.-r. Tan, X. W. Zhang, Z. Hong and Y. Yang, *ACS Nano*, 2011, **5**, 6210-6217.
17. D. Zhang, W. C. H. Choy, F. Xie, W. E. I. Sha, X. Li, B. Ding, K. Zhang, F. Huang and Y. Cao, *Adv. Funct. Mater.*, 2013, **23**, 4255-4261.
18. X. Li, W. C. H. Choy, L. Huo, F. Xie, W. E. I. Sha, B. Ding, X. Guo, Y. Li, J. Hou, J. You and Y. Yang, *Adv. Mater.*, 2012, **24**, 3046-3052.
19. X. Li, W. C. H. Choy, H. Lu, W. E. I. Sha and A. H. P. Ho, *Adv. Funct. Mater.*, 2013, **23**, 2728-2735.
20. M. J. Currie, J. K. Mapel, T. D. Heidel, S. Goffri and M. A. Baldo, *Science*, 2008, **321**, 226-228.
21. S. Tsoi, D. J. Broer, C. W. Bastiaansen and M. G. Debije, *Opt. Express*, 2010, **18**, A536-A543.
22. H. Jia, S. H. Zheng, C. Xu, W. B. Chen, J. C. Wang, X. F. Liu and J. R. Qiu, *Adv. Energy Mater.*, 2015, **5**, 14101041.
23. M. G. Debije and P. P. C. Verbunt, *Adv. Energy Mater.*, 2012, **2**, 12-35.
24. V. Fattori, M. Melucci, L. Ferrante, M. Zambianchi, I. Manet, W. Oberhauser, G. Giambastiani, M. Frediani, G. Giachi and N. Camaioni, *Energ. Environ. Sci.*, 2011, **4**, 2849-2853.
25. H. Hernandez-Noyola, D. H. Potterveld, R. J. Holt and S. B. Darling, *Energ. Environ. Sci.*, 2012, **5**, 5798-5802.
26. A. J. Das and K. S. Narayan, *Adv. Mater.*, 2013, **25**, 2193-2199.
27. D. Li and Y. Xia, *Adv. Mater.*, 2004, **16**, 1151-1170.
28. J.-Y. Chen, C.-C. Kuo, C.-S. Lai, W.-C. Chen and H.-L. Chen, *Macromolecules*, 2011, **44**, 2883-2892.
29. Y.-C. Chiu, Y. Chen, C.-C. Kuo, S.-H. Tung, T. Kakuchi and W.-C. Chen, *ACS Appl. Mat. Interfaces*, 2012, **4**, 3387-3395.
30. J. Song, M. Chen, M. B. Olesen, C. Wang, R. Havelund, Q. Li, E. Xie, R. Yang, P. Boggild, C. Wang, F. Besenbacher and M. Dong, *Nanoscale*, 2011, **3**, 4966-4971.
31. P. Wang, L. Zhang, Y. Xia, L. Tong, X. Xu and Y. Ying, *Nano Letters*, 2012, **12**, 3145-3150.

32. C.-C. Kuo, C.-T. Wang and W.-C. Chen, *Macromol. Mater. and Eng.*, 2008, **293**, 999-1008.
33. C.-C. Kuo, C.-H. Lin and W.-C. Chen, *Macromolecules*, 2007, **40**, 6959-6966.
34. D. He, B. Hu, Q.-F. Yao, K. Wang and S.-H. Yu, *ACS Nano*, 2009, **3**, 3993-4002.
35. W.-C. Wu, C.-L. Liu and W.-C. Chen, *Polymer*, 2006, **47**, 527-538.
36. J.-Y. Chen, H.-C. Wu, Y.-C. Chiu, C.-J. Lin, S.-H. Tung and W.-C. Chen, *Adv. Electron. Mater.*, 2015, **1**, 1400028.
37. C.-C. Shih, Y.-C. Chiu, W.-Y. Lee, J.-Y. Chen and W.-C. Chen, *Adv. Funct. Mater.*, 2015, **25**, 1511–1519.
38. S. H. Lim, J. Kim, S.-g. Lee and Y. S. Kim, *Chem. Commun.*, 2010, **46**, 3961-3963.
39. B. Wu, X. Wu, C. Guan, K. Fai Tai, E. K. L. Yeow, H. Jin Fan, N. Mathews and T. C. Sum, *Nat Commun*, 2013, **4**.
40. Y. Sun, Y. Yin, B. T. Mayers, T. Herricks and Y. Xia, *Chem. Mater.*, 2002, **14**, 4736-4745.
41. Y. Sun, B. Mayers, T. Herricks and Y. Xia, *Nano Letters*, 2003, **3**, 955-960.
42. Y. Sun and Y. Xia, *Adv. Mater.*, 2002, **14**, 833-837.
43. E. Braun, Y. Eichen, U. Sivan and G. Ben-Yoseph, *Nature*, 1998, **391**, 775-778.
44. S. Schietinger, T. Aichele, H.-Q. Wang, T. Nann and O. Benson, *Nano Lett.*, 2009, **10**, 134-138.
45. Q.-C. Sun, H. Mundoor, J. C. Ribot, V. Singh, I. I. Smalyukh and P. Nagpal, *Nano Lett.*, 2013, **14**, 101-106.

Table 1. OPV characteristics without or with the plasmonic-enhanced LSC ES nanofibers.

Device	V_{oc} (V)	J_{sc} (mA cm^{-2})	FF (-)	PCE[a)] (%)
P3HT:$PC_{61}BM$				
Reference [b)]	0.63	8.21	0.675	3.49±0.07
A-PFBTNF-LO	0.62	8.92	0.669	3.70±0.03
A-PFBTNF-HI	0.63	9.40	0.668	3.96±0.07
C-PFBTNF-HI	0.63	8.57	0.656	3.54±0.09
C-AgNF	0.63	8.82	0.691	3.84±0.06
C-PFBT-LO/AgNF	0.62	9.43	0.681	3.98±0.08
A-PFBT-HI/AgNF	0.63	9.40	0.690	4.09±0.06
C-PFBT-HI/AgNF	0.63	9.45	0.691	4.11±0.09
PTB7:$PC_{71}BM$				
Reference [b)]	0.76	12.07	0.659	6.05±0.09
A-PFBTNF-LO	0.75	12.75	0.660	6.31±0.06
A-PFBTNF-HI	0.76	12.84	0.671	6.55±0.10
C-AgNF	0.76	12.91	0.660	6.44±0.03
C-PFBT-LO/AgNF	0.76	13.04	0.669	6.63±0.09
C-PFBT-HI/AgNF	0.76	13.88	0.675	7.12±0.06

[a)] The average value of PCE is calculated from at least 10 cells. [b)] The reference device is the device without ES nanofibers. The abbreviations of A- and C- are the ES nanofibers with the architectures of aligned- and crossed- patterns, respectively.

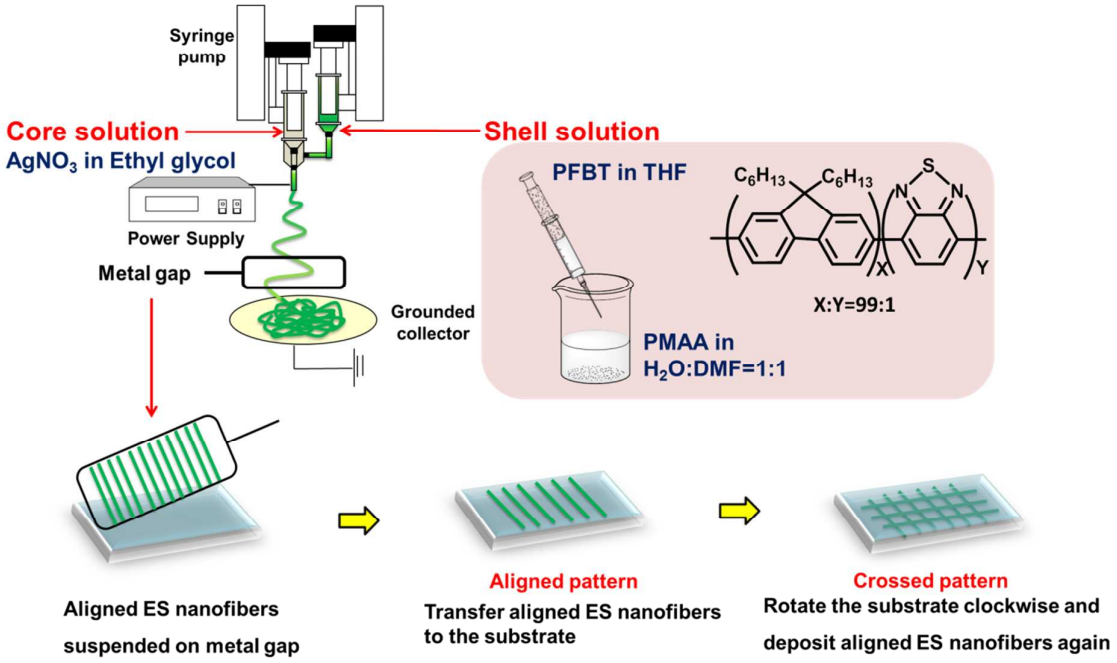

Fig. 1 Schematic representation of the coaxial electrospinning setup and the preparation of the aligned- and crossed-fiber patterns.

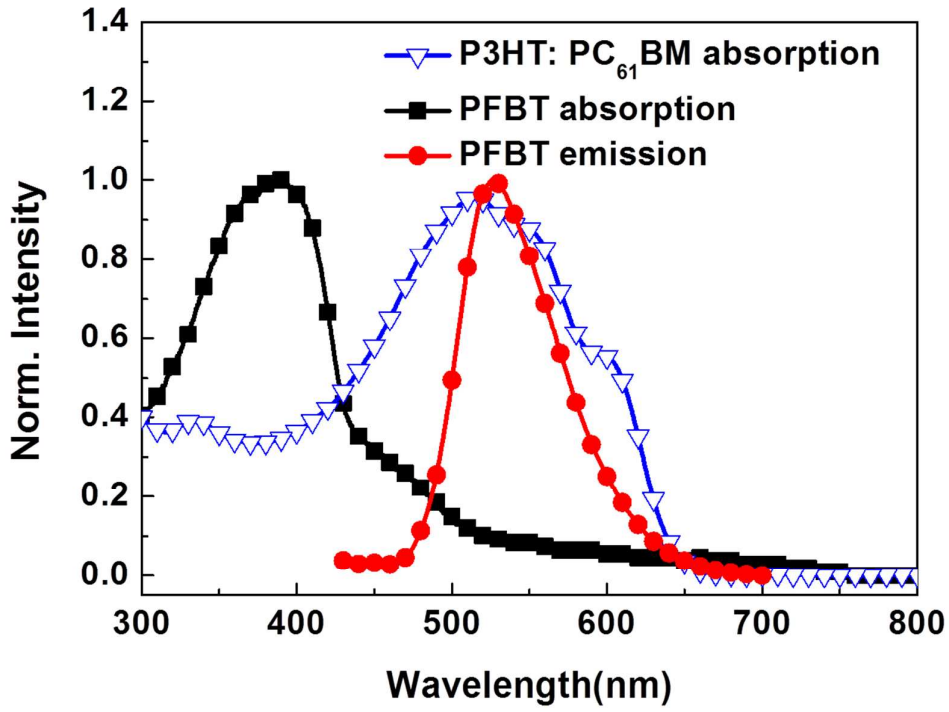

Fig. 2 Optical absorption spectra of PFBT and P3HT:$PC_{61}BM$ with corresponding emission of PFBT.

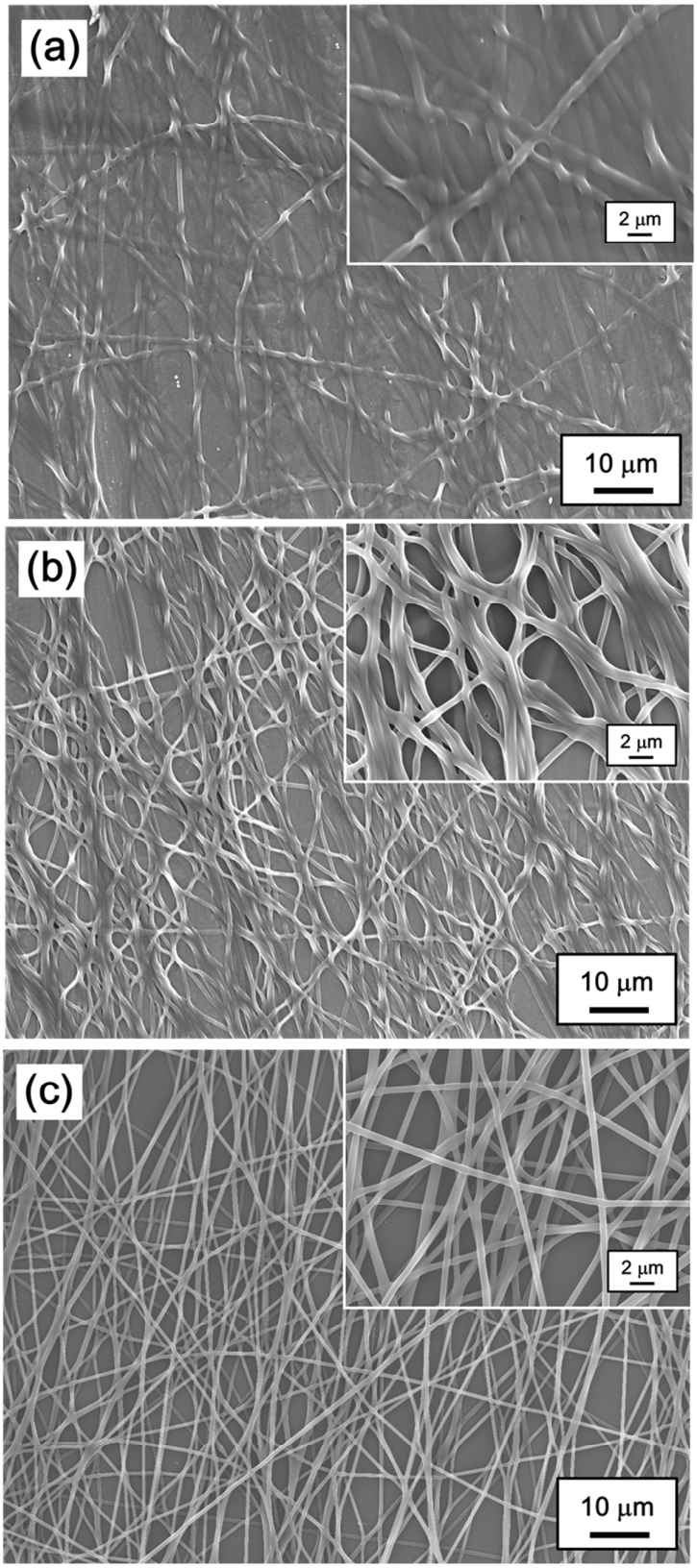

Fig. 3 FE-SEM images of the cross-linked PFBTNF-HI with different crosslinking time: (a) 5 min, (b) 10 min and (c) 20 min and treated by water .

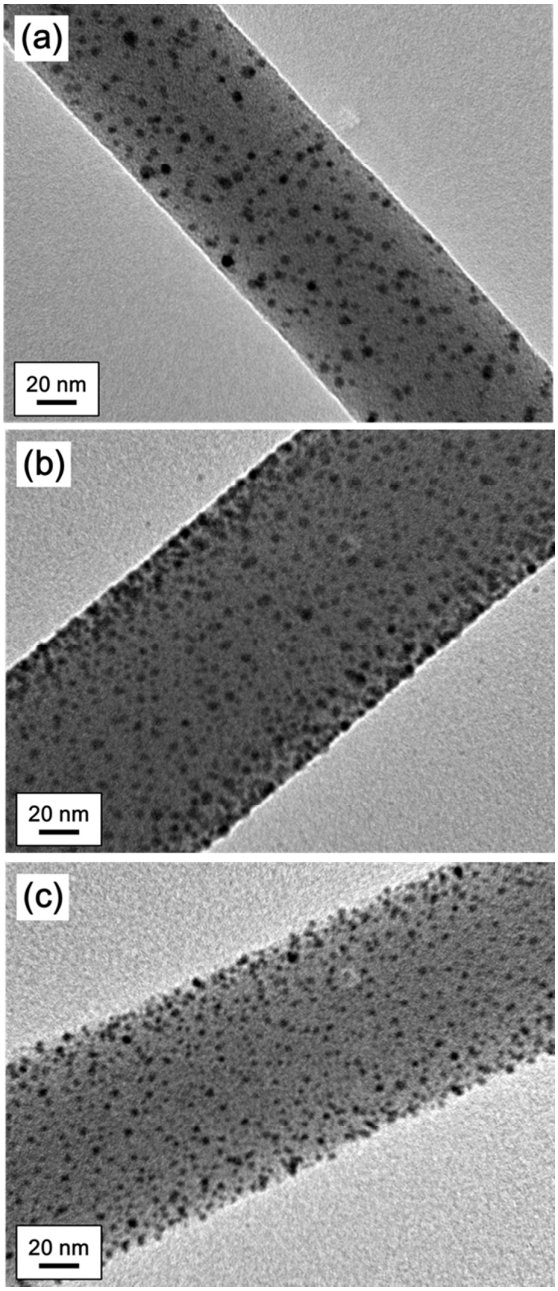

Fig. 4 TEM images of the prepared single ES nanofibers: (a) PFBTNF-HI (b) AgNF and (c) PFBT-HI/AgNF.

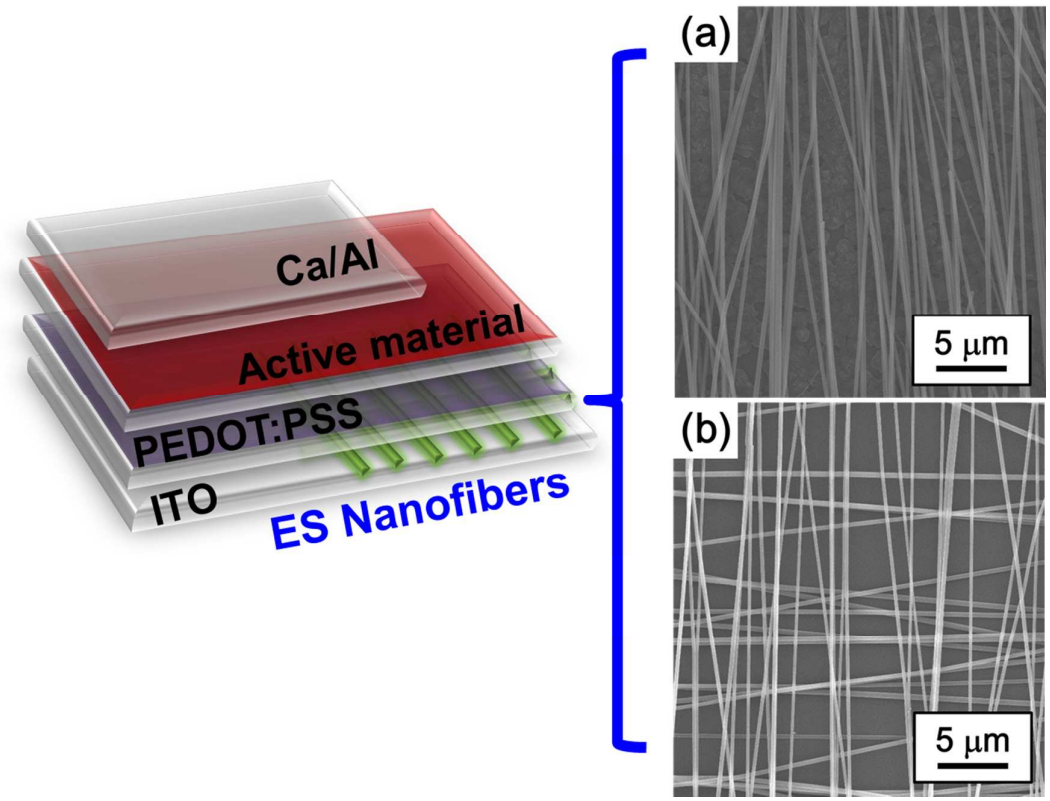

Fig. 5 Device structure of OPV cells and SEM images of PFBTNF-HI with (a) aligned- and (b) crossed-fiber patterns.

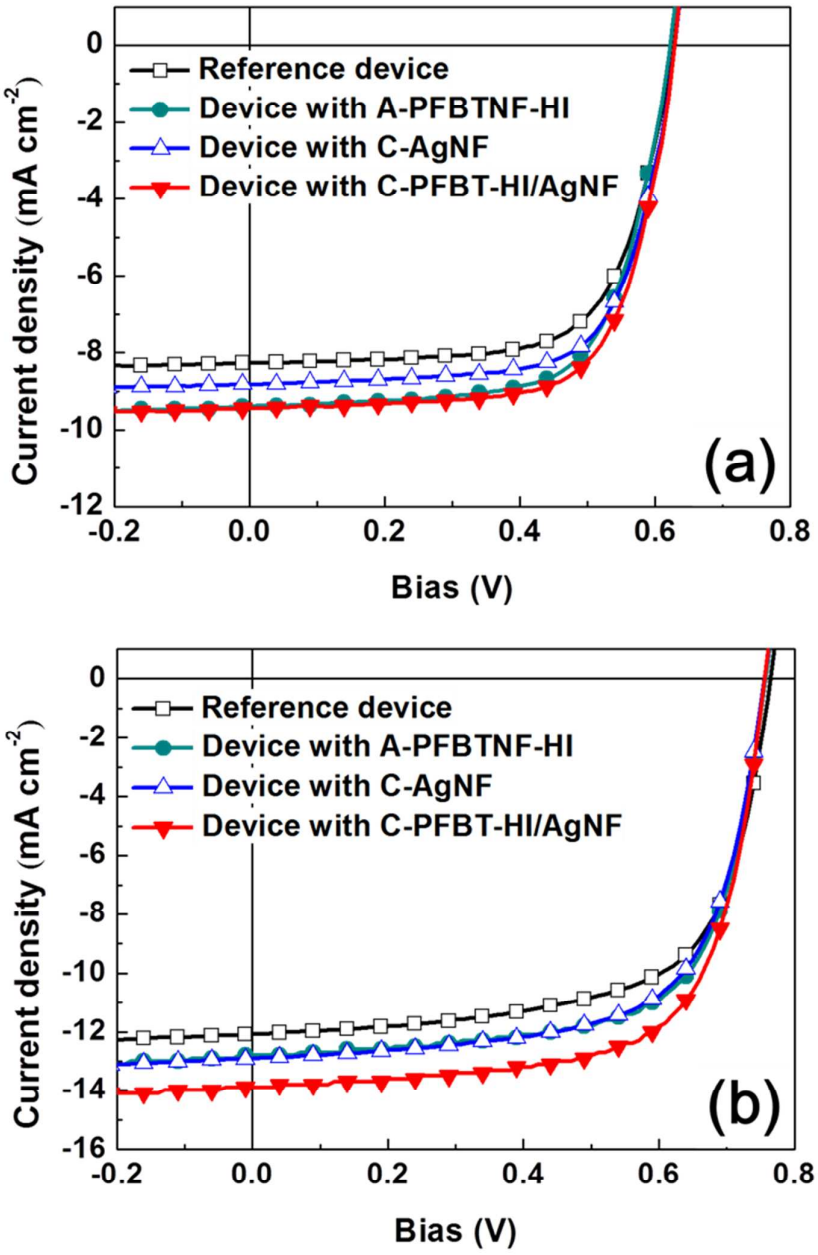

Fig. 6 (a) *J-V* characteristics of the P3HT:$PC_{61}BM$ OPV reference device, and those with A-PFBTNF-HI, C-AgNF and C-PFBT-HI/AgNF, respecitvely; (b) *J-V* characteristics of PTB7:$PC_{71}BM$ OPV reference device, and those with A-PFBTNF-HI, C-AgNF and C-PFBT-HI/AgNF, respecitvely.

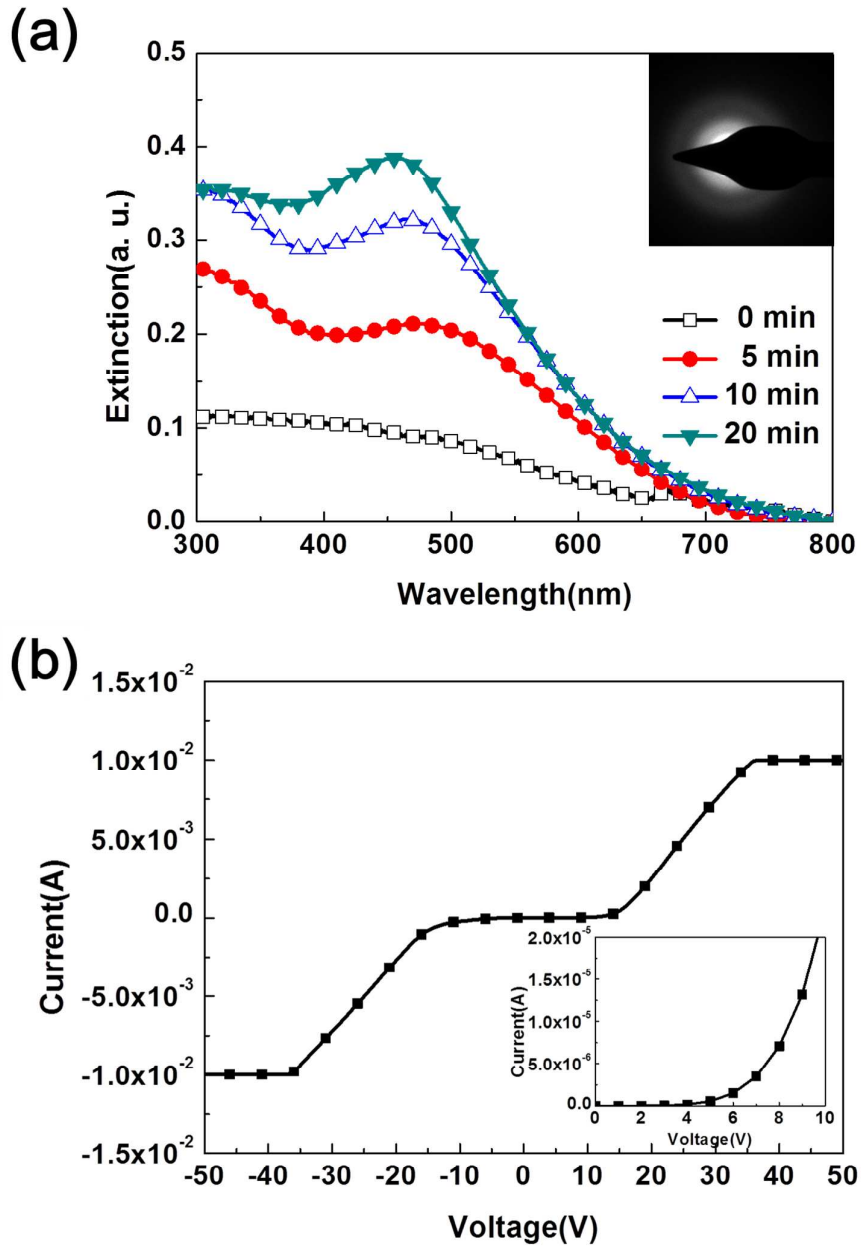

Fig. 7 (a)Temporal optical absorption spectra based on AgNF. The inset Fig. show the SAED of corresponding AgNF. (b) *I-V* characteristic of AgNF.

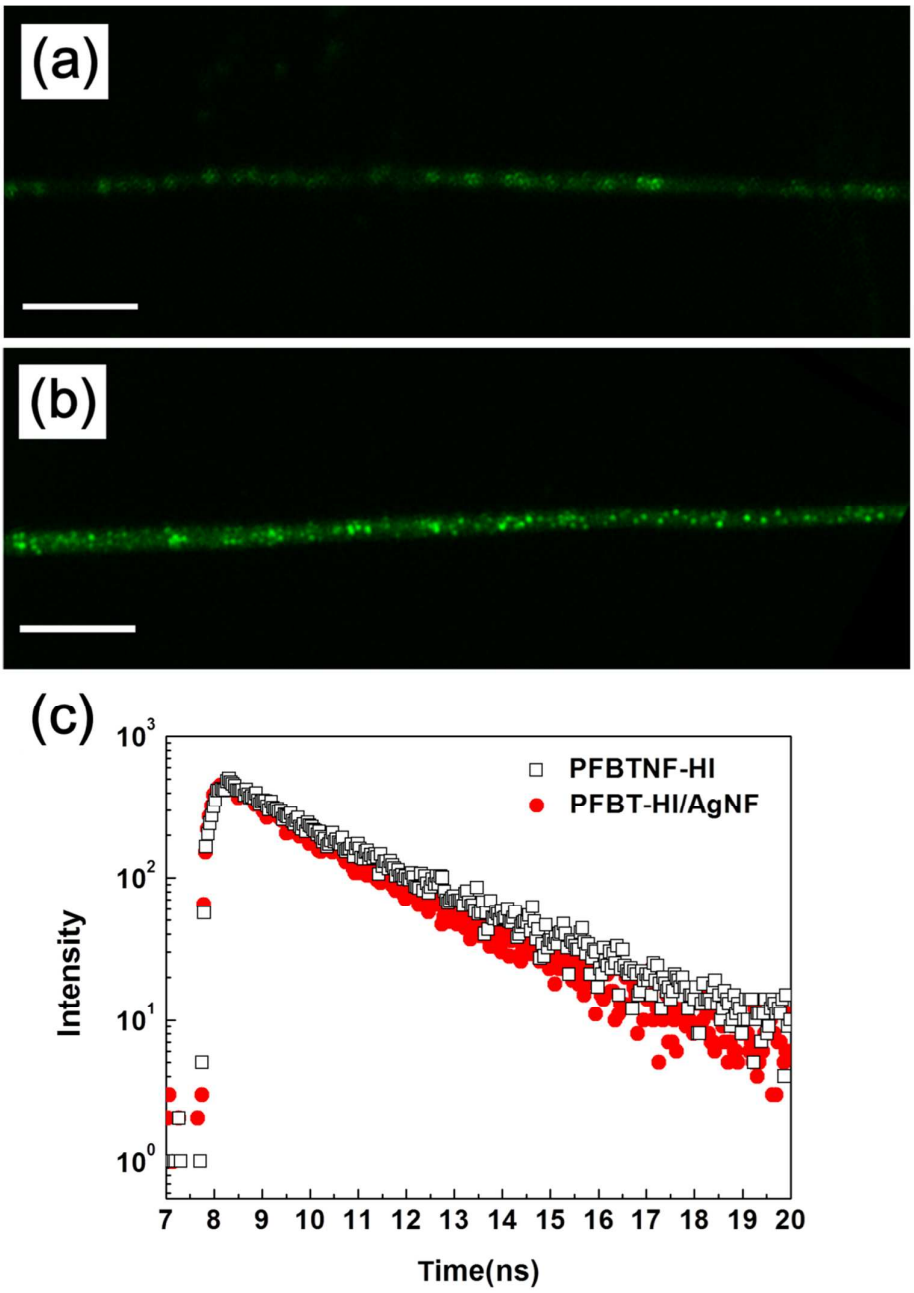

Fig. 8 Confocal image of (a) PFBTNF-HI and (b) PFBT-HI/AgNF with scale bar of 10 μm; (c) time-resolved PL of PFBTNF-HI and PFBT-HI/AgNF.

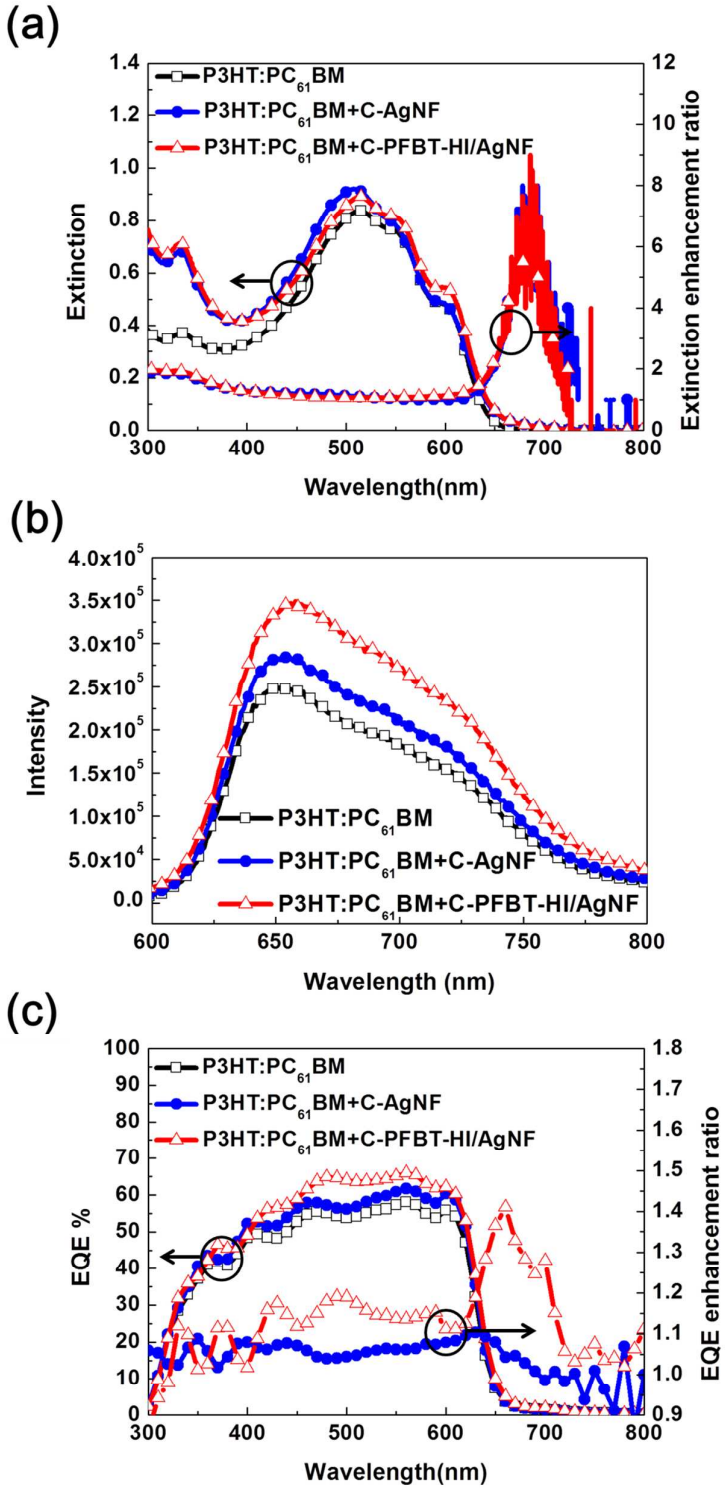

Fig. 9 (a) Extinction spectra of P3HT:PC_{61}BM, P3HT:PC_{61}BM with C-AgNF and C-PFBT-HI/AgNF. (b) EQE of P3HT:PC_{61}BM, P3HT:PC_{61}BM with C-AgNF and C-PFBT-HI/AgNF. (c) PL spectra of P3HT:PC_{61}BM, P3HT:PC_{61}BM with C-AgNF and C-PFBT-HI/AgNF.

The Dual Functional Electrospun Nanofibers with the Conbination of Luminescent Solar concentrator (LSC) using conjugated polymer nanoparticles and surface plasmon resonance (SPR) using silver nanoparticle were successfully fabricated. As the plasmonic-enhanced LSC electrospun nanofibers with a crossed pattern were employed into P3H:$PC_{61}BM$ and PTB7:$PC_{71}BM$, the power conversion efficiencies led to remarkably 18 % enhancement without sacrificing the coverage area of active layer.

Electrospun Nanofibers with Dual Plasmonic –Enhanced Luminescent Solar Concentrator Effects for High-Performance Organic Photovoltaic Cells

Jung-Yao Chen, Yu-Cheng Chiu, Chien-Chung Shih, Wen-Chung Wu, and Wen-Chang Chen*